

Radiative decay and electromagnetic moments in ^{229}Th determined within nuclear DFT

A. Restrepo-Giraldo¹, J. Dobaczewski^{1,2}, J. Bonnard¹ and X. Sun¹

¹*School of Physics, Engineering and Technology,
University of York, Heslington, York YO10 5DD, United Kingdom*

²*Institute of Theoretical Physics, Faculty of Physics,
University of Warsaw, ul. Pasteura 5, PL-02-093 Warsaw, Poland*

(Dated: February 17, 2026)

Using the nuclear DFT approach with symmetry breaking and restoration, we investigate the electromagnetic properties of the ground and isomeric states in ^{229}Th . We determine the magnetic dipole transition strength $B(M1:3/2_1^+ \rightarrow 5/2_1^+)$ between these two states and discuss the effects of parity breaking, configuration mixing, and time-odd core polarization. We also determine the corresponding spectroscopic magnetic dipole and electric quadrupole moments. Because the octupole deformability of the Skyrme functionals used here is not described in sufficient detail, we analyze the results using a set of Skyrme functionals, implementing a regression aligned with the measured octupole moments of neighboring even-even nuclei. Without parameter adjustment, the results compare favorably with the experimental data but also indicate the need to systematically adjust the octupole degrees of freedom in future functional parametrizations.

Introduction—Since the discovery of the nearly degenerate excited and ground states of ^{229}Th almost fifty years ago, many efforts have been undertaken by both experimental and theoretical communities to understand and characterize this unusual emergent feature. To date, it is the lowest excited state in the entire nuclear chart, making it a distinctive isomer of interest for experiments, theory, and potential technological applications [1–7]. Such an unusual property also makes it a difficult case to study, testing the limits of experimental and theoretical methods.

Its first detection comes from the γ -spectrum of the α -decaying ^{233}U , where an excited state with energy below 100 eV was proposed to explain its decay scheme [8]. Several subsequent spectroscopic studies helped clarify the excited state and further constrained its energy [9–13]. Later, direct detection of internal conversion electrons allowed for a more precise characterization of the isomeric state [14]. Since then, alternative production channels and measurement techniques have been developed to accurately determine the values of its decay properties, including electromagnetic moments [15–19] and to study internal conversion processes from excited electronic configurations [20].

Because of the low energy of the radiative transition, the electronic environment strongly influences its properties, making lifetime measurements depend on specific experimental setups and requiring corrections to estimate the corresponding vacuum transition rates. The latest results [21] report a transition energy of $E_\gamma = 8.35574(3)$ eV, a half-life in vacuum of $t_{1/2} = 1740(50)$ s, and a corresponding reduced transition probability of $B(M1)=0.0217(6)$ W.u._{M1} = $0.0388(12)$ μ_N^2 [22], marking a significant improvement in precision compared to previous studies as shown in [23]. Note that 1 W.u._{M1} = 1.7905 μ_N^2 .

The electromagnetic moments have been measured for both the $3/2^+$ isomeric and $5/2^+$ ground states [24–27]. The latest measurements of spectroscopic electric quadrupole moments are $Q(3/2^+) = 1.77(1)$ b and $Q(5/2^+) = 3.11(2)$ b [6]. For the magnetic dipole moments, the latest reports are $\mu(3/2^+) = -0.378(8)$ μ_N and $\mu(5/2^+) = 0.366(6)$ μ_N [28]. The deviation from the Schmidt limits [29] $\mu_{\text{Sch.}}(5/2) = [1.366, -1.913]$ μ_N and $\mu_{\text{Sch.}}(3/2) = [1.148, -1.913]$ μ_N indicate a strong core polarization effect in this isotope.

The advances in the experimental field have been motivated by prospective technological applications in areas like chronometry [30–34], γ -ray laser technology [35, 36], satellite-based navigational, and chronological geodesy systems [3]. These developments have the potential to enhance a new generation of ultra-precise techniques that will eventually also advance scientific research [2, 5, 6]. However, such developments depend on precise control of the excitation and de-excitation processes between the $3/2^+$ state and the $5/2^+$ ground state, where M1 multipolarity greatly exceeds the competing E2 by about 10^{13} orders of magnitude due to the extremely low energy of the transition [37]. Recent advancements have achieved the first optical-controlled laser excitation in doped crystals of $\text{Th}:\text{CaF}_2$ and $\text{Th}:\text{LiSrAlF}_6$ along with new proposals being currently developed, demonstrating that these applications are feasible [21, 38–41].

Theoretical efforts to understand and predict the observables of this elusive isomeric transition have been done in the frameworks of phenomenological [37], core-plus-particle [11, 13, 42–45], and projected shell models [46]. In these approaches, reliance on adjusted parameters, effective charges, or effective g factors was crucial for accurately reproducing observables. Previous parameter-free self-consistent approaches have been implemented without parity breaking, that is, neglecting

the octupole deformation [2], time-reversal and signature symmetry breaking, which preclude angular-momentum core polarisation [2, 47], parity and rotational symmetry restoration [2, 48], or configuration interaction [2, 47, 48] to obtain low-energy structure, multipole moments, and transition strengths.

In this Letter, we present the first parameter-free analysis based on self-consistent nuclear density functional theory (DFT) that incorporates all previously missing elements and employs the methodology of Refs. [49, 50] predating the lifetime measurement [21]; see also Refs. [51–53]. We apply the configuration-interaction multi-reference DFT (MR-DFT) approach with several Skyrme functionals, mixing two sets of paired, octupole-deformed, and symmetry-restored configurations, one for the ground state and the other for the isomer, and estimate the corresponding B(M1) value and electromagnetic moments. A similar configuration-interaction approach has recently been successfully used to calculate two-neutrino double-beta decay matrix elements [54].

Method—We conducted a multi-step calculation of the ground and isomeric nuclear wave functions of ^{229}Th to determine the magnetic dipole transition strength $B(\text{M}1:3/2_1^+ \rightarrow 5/2_1^+)$ and the electromagnetic moments $Q(3/2^+)$, $Q(5/2^+)$, $\mu(3/2^+)$ and $\mu(5/2^+)$ for several Skyrme functionals with pairing interaction, implemented in the code HFODD [55–57] version 3.33k. We used the pairing strengths, $V_{0,n}$ and $V_{0,p}$, from Ref. [58] that reproduce the mass staggering around ^{229}Th and ^{227}Ac , respectively, and the Landau parameters g'_0 [59, 60] from Refs. [49, 59] that constrain the isovector spin-spin coupling constants; see the End Matter. We present results using seven Skyrme functionals: SkX_c [61], SkM* [62], UNEDF1 [63], SIII [64], SkO' [65], SLy4 [66], and UNEDF0 [67].

Since none of these Skyrme functionals was adjusted to data on octupole degrees of freedom, we anticipated systematic disagreement among the calculations. Therefore, following Ref. [68], we analyzed correlations between the calculated intrinsic octupole moments Q_0^3 and the predicted B(M1) and electromagnetic moments, using the experimental values of Q_0^3 as reference points. To this end, we computed the ground-state octupole moments of ^{226}Ra and ^{230}Th and used the experimental values [69] for these isotopes, $Q_0^3(^{226}\text{Ra}) = 1080(30) \text{ e fm}^3$ [70, 71] and $Q_0^3(^{230}\text{Th}) = 800(40) \text{ e fm}^3$ [72].

Our computational approach involved blocking specific odd-neutron axial quasiparticle configurations in ^{229}Th and relaxing parity constraints. This yielded deformed, symmetry-breaking solutions with non-zero intrinsic octupole moments Q_0^3 . We then projected these solutions onto good parity and angular momentum and mixed them.

As discussed in Ref. [53] and in references cited therein, the DFT magnetic moments critically depend on the so-called time-odd (TO) terms of the mean field [73–75],

which are solely responsible for the angular-momentum polarization of the core. To assess their role in determining the M1 transition rates, we performed all calculations in two variants: (i) with the time-even (TE) terms only and (ii) with both TE and TO terms included. In addition, the TE+TO results were obtained for the isovector spin-spin terms of the functionals, with consistent Landau parameters [59, 60] either adjusted to experimental magnetic moments [49] or to the Gamow-Teller strengths [59]; see the End Matter.

Procedure—Here, we describe the multi-step process used to determine the results of this study. First, for each Skyrme functional, we determined the axial-parity-breaking paired ground-state wave functions of the neighboring even-even isotope ^{228}Th , from which we obtained the corresponding single-particle (s.p.) wave functions. Then, for each of the angular-momentum projections along the axis of axial symmetry, $\Omega = 5/2$ and $\Omega = 3/2$, we selected three of them near the Fermi surface to be blocked [76–78] in the odd- N isotope ^{229}Th .

In the second step, the ^{228}Th s.p. wave functions served as tags to self-consistently determine the quasiparticle configurations in ^{229}Th , as explained in Ref. [51]. To establish a common naming convention for those configurations, we use the calculated dominant Nilsson labels [79] of the ^{228}Th tag states, which, following Ref. [52], we denote with parentheses instead of brackets. They are (642)3/2, (741)3/2, and (631)3/2 for $\Omega = 3/2$ and (633)5/2, (752)5/2, and (622)5/2 for $\Omega = 5/2$. Note that we also consider parity-broken configurations with Nilsson labels of $N_0 = 7$, as they may acquire positive-parity components after parity restoration.

The tagging technology enables tracking of blocked quasiparticle states throughout the self-consistent iterations, regardless of their changing energies and deformations. In this way, we obtained the self-consistent symmetry-broken ^{229}Th wave functions $|\Phi_{n\Omega}\rangle$ for the three lowest configurations, $n = 1, 2, 3$, of $\Omega = 5/2$ and $\Omega = 3/2$. In some cases, the Nilsson labels of the blocked self-consistent quasiparticle orbitals can differ from those of the tag states, which may occur when the dominance of a given Nilsson state $[N_0 n_z \Lambda] \Omega$ is not very strong, as discussed in Ref. [53].

Then, in the third step, we restored broken symmetries [80] by projecting wave functions $|\Phi_{n\Omega}\rangle$ onto good angular momentum I and positive parity $\pi = +$. We denote the resulting band-head wave functions ($I = |\Omega|$) as $|\Phi_{nI+\Omega}\rangle$, that is, $|\Phi_{n5/2+5/2}\rangle$ and $|\Phi_{n3/2+3/2}\rangle$. Previous tests have shown [51] that particle-number restoration does not affect magnetic moments. Because it increases computation time by two orders of magnitude, we did not perform it in this study.

In the fourth step, we calculated two sets of 3×3 matrix elements of the Hamiltonian $H_{nn'}^{I+\Omega} = \langle \Phi_{nI+\Omega} | \hat{H} | \Phi_{n'I+\Omega} \rangle$ and the overlap $N_{nn'}^{I+\Omega} = \langle \Phi_{nI+\Omega} | \Phi_{n'I+\Omega} \rangle$ for $I = \Omega = 5/2$ and $I = \Omega = 3/2$, along with the set of

6×6 M1 matrix elements of the magnetic dipole \hat{M} , $M_{nn'}^{II'} = \langle \Phi_{nI+I} | \hat{M} | \Phi_{n'I'+I'} \rangle$, and the electric quadrupole \hat{Q} , $Q_{nn'}^{II'} = \langle \Phi_{nI+I} | \hat{Q} | \Phi_{n'I'+I'} \rangle$. For the Skyrme functionals, the matrix elements of the Hamiltonian were determined using the standard methodology defined in the generator coordinate method [75, 76].

Next, in the fifth step, for $I^\pi = 5/2^+$ and $I^\pi = 3/2^+$, we solved two configuration-interaction equations (the Hill-Wheeler equations [75, 76]),

$$\sum_{n'} H_{nn'}^{I^+\Omega} a_{n'I+\Omega} = E \sum_{n'} N_{nn'}^{I^+\Omega} a_{n'I+\Omega}, \quad (1)$$

where we considered only the solutions with the lowest energies, E . This yielded the mixing coefficients $a_{n'I+\Omega}$ and the normalized mixed wave functions $|\Phi_{I+\Omega}\rangle = \sum_{n'} a_{n'I+\Omega} |\Phi_{n'I+\Omega}\rangle$. We note that the states $|\Phi_{n'I+\Omega}\rangle$ are generally non-orthogonal ($N_{nn'}^{I^+\Omega} \neq \delta_{nn'}$); therefore, the mixing coefficients $a_{n'I+\Omega}$ cannot be interpreted as probability amplitudes.

In the final sixth step, we could then determine the MR-DFT matrix element of the M1 transition between the $I^\pi = 5/2^+$ and $I^\pi = 3/2^+$ states,

$$\langle \Phi_{5/2+5/2} | \hat{M} | \Phi_{3/2+3/2} \rangle = \sum_{nn'} a_{n5/2+5/2}^* M_{nn'}^{5/2\ 3/2} a_{n'3/2+3/2}, \quad (2)$$

and the corresponding reduced transition probability,

$$B(\text{M1} : 3/2_1^+ \rightarrow 5/2_1^+) = \frac{1}{4} |\langle \Phi_{5/2+5/2} | \hat{M} | \Phi_{3/2+3/2} \rangle|^2. \quad (3)$$

Similarly, we determine the spectroscopic electromagnetic moments of the $I^\pi = 5/2^+$ and $I^\pi = 3/2^+$ states as follows,

$$\langle \Phi_{I+I} | \hat{M} | \Phi_{I+I} \rangle = \sum_{nn'} a_{nI+I}^* M_{nn'}^{II} a_{n'I+I}, \quad (4)$$

$$\langle \Phi_{I+I} | \hat{Q} | \Phi_{I+I} \rangle = \sum_{nn'} a_{nI+I}^* Q_{nn'}^{II} a_{n'I+I}. \quad (5)$$

Results—Figure 1 presents our study's principal findings. It compares the TE B(M1) values (upper panels) with the TE+TO values (lower panels) derived from the measured intrinsic octupole moments in ^{226}Ra (left panels) and ^{230}Th (right panels). In each case, results for different Skyrme functionals were analyzed using the linear regression method of Ref. [68] and extrapolated, with uncertainties, to the measured points.

Encouragingly, the TE+TO results extrapolated to the experimental data for ^{226}Ra and ^{230}Th are consistent with each other, yielding $B(\text{M1})=0.04(3)$ and $0.03(2) \mu_N^2$, respectively. It is also gratifying that both agree with the experimental value of $0.0388(12) \mu_N^2$ [21] (uncertainties calculated from error propagation). However, the large spread in results obtained with different Skyrme functionals leads to a theoretical uncertainty that is much larger than the experimental uncertainty.

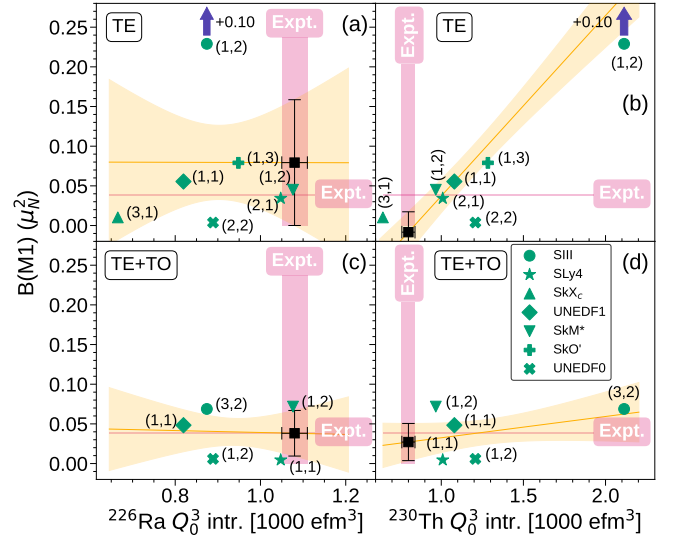


FIG. 1. $B(\text{M1})$ values with respect to the intrinsic octupole moments Q_0^3 of ^{226}Ra (left panels) and ^{230}Th (right panels), determined for functionals reduced to the time-even mean fields (TE, upper panels) and with complete time-even and time-odd mean fields (TE+TO, lower panels). The numbers in parentheses indicate the number of successfully mixed wave functions for the two configurations, namely $(5/2^+, 3/2^+)$. Vertical and horizontal stripes labelled Expt. are the experimental values of Q_0^3 and $B(\text{M1})$, respectively. Thick lines and shaded bands denote the regression results and their uncertainties, respectively [68]. Arrows denote shifted points outside the scale of the figure.

The TE results, characterized by large outlier SIII values, read $B(\text{M1})=0.08(8)$ and $-0.01(3) \mu_N^2$, respectively. They are less compatible with experiment, less consistent with one another, and may exhibit greater uncertainty. The current results thus provide some indication of the importance of time-odd mean fields in describing the $B(\text{M1})$ value in ^{229}Th .

The main challenge in obtaining the results shown in Fig. 1 is that the Hamiltonian mixing matrix elements $H_{nn'}^{I^+\Omega}$ are often singular due to non-zero self-interaction and self-pairing energies that characterize Skyrme functionals (see discussion in Ref. [80]). This problem has not been satisfactorily resolved yet, although the search for a solution continues [81–83]. In this work, we removed all singular cases from the analysis (see the End Matter), and the number retained is shown in parentheses in Fig. 1.

As shown in Fig. 2, configuration interaction has a limited effect on the $B(\text{M1})$ values. The figure shows values calculated for only one $3/2^+$ configuration [631]3/2 and one $5/2^+$ configuration [633]5/2. For the TE+TO option, the results are nearly identical to those obtained with the mixed configurations. However, we had to discard all points that did not converge properly; see the End Matter.

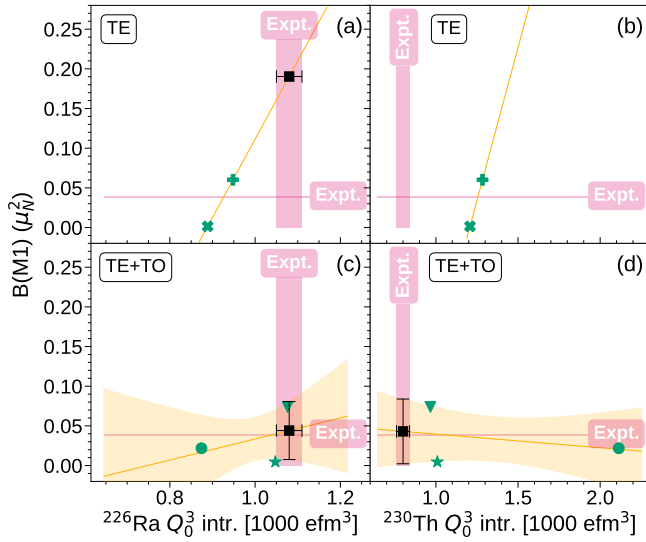


FIG. 2. Same as in Fig. 1 but for the $B(M1)$ values calculated between converged individual (not mixed) blocked self-consistent states $[631]3/2$ and $[633]5/2$.

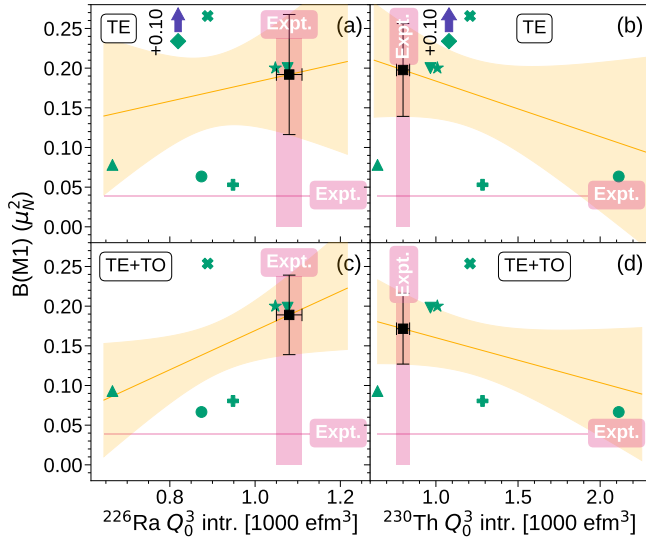


FIG. 3. Same as in Fig. 2 but for the $B(M1)$ values calculated between parity-conserving states.

Finally, in Fig. 3, we present results obtained by preserving the parity of the $[631]3/2$ and $[633]5/2$ states in ^{229}Th . Neglecting the octupole deformation leads to a significant discrepancy with the experimental $B(M1)$ value and is therefore unacceptable.

Figure 4(a) compares all the $B(M1)$ results discussed above with the experimental value; the corresponding numerical results are given in the End Matter. To benchmark our methods against other experimentally known electromagnetic observables in ^{229}Th , panels (b)–(e) of Fig. 4 summarize results for the magnetic dipole moments, plotted on an absolute scale in panels (b)

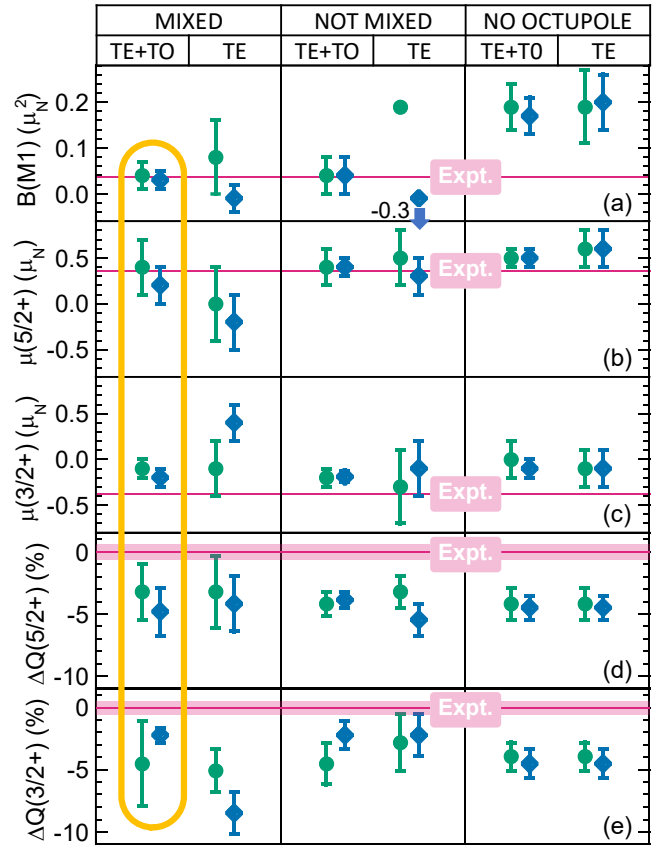


FIG. 4. Summary results obtained in this Letter, compared with the experimental data [6, 21, 28]. The shown values are: reduced transition probabilities $B(M1)$ (a), magnetic dipole moments of the $5/2^+$ (b) and $3/2^+$ (c) states, and electric quadrupole moments of the $5/2^+$ (d) and $3/2^+$ (e) states. Circles and diamonds correspond to the regression aligned with the measured octupole moments of ^{226}Ra and ^{230}Th , respectively.

and (c), and the electric quadrupole moments, plotted on a percentage-deviation scale, $\Delta Q = (Q_{\text{DFT}} - Q_{\text{Expt}})/Q_{\text{Expt}}$, in panels (d) and (e). We observe that the moments of both the $5/2^+$ and $3/2^+$ states do not strongly depend on the version of our calculation, but are, nevertheless, closest to the data for the most advanced version, denoted by the oval in Fig. 4. The magnetic moment of the $5/2^+$ ground state is well reproduced, whereas that of the isomer $3/2^+$ is underestimated by about a factor of two. However, this disagreement does not impede the accurate reproduction of the $B(M1)$ value in panel (a). On the other hand, the quadrupole moments of both states are reproduced very well; calculations underestimate the data by only a few percent. Detailed plots showing the regression analyses for the electromagnetic moments are collected in the Supplemental Material [84].

Conclusions—We presented the first application of nuclear DFT to the challenging problem of describing the

electromagnetic properties of ^{229}Th , including the decay rate of its low-energy isomer. We addressed three fundamental questions in describing these properties: the role of configuration interaction, time-odd core polarization, and octupole correlations. Since the configurations of the isomer and ground state can be confidently based on two distinct deformed neutron orbitals, the main physics aspects of the problem concern details of their structure. Our results indicate that the role of configuration interaction is probably small, that of time-odd polarization is significant, and that including the effects of octupole correlations is fundamental. We reached these conclusions within a theory that allows symmetry breaking while fully respecting symmetry restoration.

The consistent description of the data obtained without parameter adjustments is gratifying. Still, the crucial need to properly account for octupole correlations points to the most essential way to improve the approach's predictive power: fine-tuning the functional's octupole polarizability within global adjustments to experimental data. In practice, there is also a fundamental drawback to the existing functionals, which all struggle with self-interactions and self-pairing, rendering many applications erratic and unacceptable. An intensified effort in these two directions is strongly warranted.

We thank Herlik Wibowo for fruitful discussions and Pierre Becker and Alessandro Pastore for their early involvement in the project. COLFUTURO financially supported ARG. This work was partially supported by the STFC Grant Nos. ST/V001035/1 and ST/Y000285/1, and by a Leverhulme Trust Research Project Grant. We thank the CSC-IT Center for Science Ltd., Finland, and the IFT Computer Center at the University of Warsaw, Poland, for the allocation of computational resources. This project was partly undertaken on the Viking Cluster, a high-performance compute facility provided by the University of York. We are grateful for computational support from the University of York High Performance Computing service, Viking, and the Research Computing team. We thank Grammarly for its support with English writing.

Data availability—The data that support the findings of this article are openly available [85].

[1] X.-t. He and Z.-z. Ren, Enhanced sensitivity to variation of fundamental constants in the transitions of ^{229}Th and ^{249}Bk , *Journal of Physics G: Nuclear and Particle Physics* **34**, 1611 (2007).
 [2] E. Litvinova, H. Feldmeier, J. Dobaczewski, and V. Flambaum, Nuclear structure of lowest ^{229}Th states and time-dependent fundamental constants, *Phys. Rev. C* **79**, 064303 (2009).
 [3] P. G. Thirolf, B. Seiferle, and L. von der Wense, The 229-thorium isomer: doorway to the road from the atomic

clock to the nuclear clock, *Journal of Physics B: Atomic, Molecular and Optical Physics* **52**, 203001 (2019).
 [4] A. Caputo, D. Gazit, H.-W. Hammer, J. Kopp, G. Paz, G. Perez, and K. Springmann, Sensitivity of nuclear clocks to new physics, *Phys. Rev. C* **112**, L031302 (2025).
 [5] E. Fuchs, F. Kirk, E. Madge, C. Paranjape, E. Peik, G. Perez, W. Ratzinger, and J. Tiedau, Searching for dark matter with the ^{229}Th nuclear lineshape from laser spectroscopy, *Phys. Rev. X* **15**, 021055 (2025).
 [6] K. Beeks, G. A. Kazakov, F. Schaden, I. Morawetz, L. Toscani De Col, T. Riebner, M. Bartokos, T. Sikorsky, T. Schumm, C. Zhang, T. Ooi, J. S. Higgins, J. F. Doyle, J. Ye, and M. S. Safronova, Fine-structure constant sensitivity of the Th-229 nuclear clock transition, *Nature Communications* **16**, 9147 (2025).
 [7] X. tao He and Z. zhou Ren, Temporal variation of the fine structure constant and the strong interaction parameter in the ^{229}Th transition, *Nuclear Physics A* **806**, 117 (2008).
 [8] L. Kroger and C. Reich, Features of the low-energy level scheme of ^{229}Th as observed in the α -decay of ^{233}U , *Nuclear Physics A* **259**, 29 (1976).
 [9] R. G. Helmer and C. W. Reich, An excited state of ^{229}Th at 3.5 eV, *Phys. Rev. C* **49**, 1845 (1994).
 [10] E. Peik and C. Tamm, Nuclear laser spectroscopy of the 3.5 eV transition in Th-229, *Europhysics Letters* **61**, 181 (2003).
 [11] E. Ruchowska, W. A. Plóciennik, J. Żylicz, H. Mach, J. Kvasil, A. Algora, N. Amzal, T. Bäck, M. G. Borge, R. Boutami, P. A. Butler, J. Cederkäll, B. Cederwall, B. Fogelberg, L. M. Fraile, H. O. U. Fynbo, E. Hagebø, P. Hoff, H. Gausemel, A. Jungclaus, R. Kaczarowski, A. Kerek, W. Kurcewicz, K. Lagergren, E. Nacher, B. Rubio, A. Syntfeld, O. Tengblad, A. A. Wasilewski, and L. Weissman, Nuclear structure of ^{229}Th , *Phys. Rev. C* **73**, 044326 (2006).
 [12] S. Matinyan, Lasers as a bridge between atomic and nuclear physics, *Physics Reports* **298**, 199 (1998).
 [13] K. Gulda, W. Kurcewicz, A. Aas, M. Borge, D. Burke, B. Fogelberg, I. Grant, E. Hagebø, N. Kaffrell, J. Kvasil, G. Løvhøiden, H. Mach, A. Mackova, T. Martinez, G. Nyman, B. Rubio, J. Tain, O. Tengblad, and T. Thorsteinson, The nuclear structure of ^{229}Th , *Nuclear Physics A* **703**, 45 (2002).
 [14] L. von der Wense, B. Seiferle, M. Laatiaoui, J. B. Neumayr, H.-J. Maier, H.-F. Wirth, C. Mokry, J. Runke, K. Eberhardt, C. E. Düllmann, N. G. Trautmann, and P. G. Thirolf, Direct detection of the ^{229}Th nuclear clock transition, *Nature* **533**, 47 (2016).
 [15] D. Moritz, K. Scharl, M. Wiesinger, G. Holthoff, T. Teschler, M. I. Hussain, J. R. Crespo López-Urrutia, T. Dickel, S. Ding, C. E. Düllmann, E. R. Hudson, S. Kraemer, L. Löbell, C. Mokry, J. Runke, B. Seiferle, L. von der Wense, F. Zacherl, and P. G. Thirolf, A cryogenic paul trap for probing the nuclear isomeric excited state $^{m}\text{Th}^{3+}$, *The European Physical Journal D* **79**, 127 (2025).
 [16] M. Verlinde, S. Kraemer, J. Moens, K. Chrysalidis, J. G. Correia, S. Cottenier, H. De Witte, D. V. Fedorov, V. N. Fedosseev, R. Ferrer, L. M. Fraile, S. Geldhof, C. A. Granados, M. Laatiaoui, T. A. L. Lima, P.-C. Lin, V. Manea, B. A. Marsh, I. Moore, L. M. C. Pereira, S. Raeder, P. Van den Bergh, P. Van Duppen, A. Vantomme, E. Verstraelen, U. Wahl, and S. G. Wilkins, Al-

- ternative approach to populate and study the ^{229}Th nuclear clock isomer, *Phys. Rev. C* **100**, 024315 (2019).
- [17] S. Kraemer, J. Moens, M. Athanasakis-Kaklamanakis, S. Bara, K. Beeks, P. Chhetri, K. Chrysalidis, A. Claessens, T. E. Cocolios, J. G. M. Correia, H. D. Witte, R. Ferrer, S. Geldhof, R. Heinke, N. Hosseini, M. Huyse, U. Köster, Y. Kudryavtsev, M. Laatiaoui, R. Lica, G. Magchiels, V. Manea, C. Merckling, L. M. C. Pereira, S. Raeder, T. Schumm, S. Sels, P. G. Thirolf, S. M. Tunhuma, P. Van Den Bergh, P. Van Duppen, A. Vantomme, M. Verlinde, R. Villarreal, and U. Wahl, Observation of the radiative decay of the ^{229}Th nuclear clock isomer, *Nature* **617**, 706 (2023).
- [18] G. Zitzer, J. Tiedau, C. E. Dillmann, M. V. Okhupkin, and E. Peik, Laser spectroscopy on the hyperfine structure and isotope shift of sympathetically cooled $^{229}\text{Th}^{3+}$ ions, *Phys. Rev. A* **111**, L050802 (2025).
- [19] Y.-Y. Xu, Q. Xiao, J.-H. Cheng, W.-Y. Zhang, and T.-P. Yu, Charge state regulation of nuclear excitation by electron capture in ^{229}Th ions (2025), arXiv:2510.08212 [nucl-th].
- [20] P. V. Bilous, G. A. Kazakov, I. D. Moore, T. Schumm, and A. Pálffy, Internal conversion from excited electronic states of ^{229}Th ions, *Phys. Rev. A* **95**, 032503 (2017).
- [21] J. Tiedau, M. V. Okhupkin, K. Zhang, J. Thielking, G. Zitzer, E. Peik, F. Schaden, T. Pronebner, I. Morawetz, L. T. De Col, F. Schneider, A. Leitner, M. Pressler, G. A. Kazakov, K. Beeks, T. Sikorsky, and T. Schumm, Laser excitation of the Th-229 nucleus, *Phys. Rev. Lett.* **132**, 182501 (2024).
- [22] Uncertainties calculated from error propagation of the measurements of $t_{1/2}$ and E_γ .
- [23] P. Thirolf, Shedding light on the Thorium-229 nuclear clock isomer, *Physics* **17**, 71 (2024).
- [24] S. Gerstenkorn, P. Luc, J. Verges, D. W. Englekemeir, J. E. Gindler, and F. S. Tomkins, Structures hyperfines du spectre d'étincelle, moment magnétique et quadrupolaire de l'isotope ^{229}Th , *J. Phys. (Paris)* **35**, 483 (1974).
- [25] C. J. Campbell, A. G. Radnaev, and A. Kuzmich, Wigner crystals of ^{229}Th for optical excitation of the nuclear isomer, *Phys. Rev. Lett.* **106**, 223001 (2011).
- [26] M. S. Safronova, U. I. Safronova, A. G. Radnaev, C. J. Campbell, and A. Kuzmich, Magnetic dipole and electric quadrupole moments of the ^{229}Th nucleus, *Phys. Rev. A* **88**, 060501 (2013).
- [27] S. G. Porsev, M. S. Safronova, and M. G. Kozlov, Precision calculation of hyperfine constants for extracting nuclear moments of ^{229}Th , *Phys. Rev. Lett.* **127**, 253001 (2021).
- [28] A. Yamaguchi, Y. Shigekawa, H. Haba, H. Kikunaga, K. Shirasaki, M. Wada, and H. Katori, Laser spectroscopy of triply charged ^{229}Th isomer for a nuclear clock, *Nature* **629**, 62 (2024).
- [29] T. Schmidt, Über die magnetischen momente der atomkerne, *Zeitschrift für Physik* **106**, 358 (1937).
- [30] C. J. Campbell, A. G. Radnaev, A. Kuzmich, V. A. Dzuba, V. V. Flambaum, and A. Derevianko, Single-ion nuclear clock for metrology at the 19th decimal place, *Phys. Rev. Lett.* **108**, 120802 (2012).
- [31] H. W. T. Morgan, R. Elwell, J. E. S. Terhune, H. B. Tran Tan, U. C. Perera, A. Derevianko, A. N. Alexandrova, and E. R. Hudson, Proposal and theoretical investigation of ^{229}Th -doped nonlinear optical crystals for compact solid-state clocks, *Applied Physics Letters* **126**, 111101 (2025).
- [32] S. M. Girvin and L. Radzihovsky, Prospects for a solid-state nuclear clock (2025), arXiv:2511.13017 [physics.atom-ph].
- [33] T. Masuda, A. Yoshimi, A. Fujieda, H. Fujimoto, H. Haba, H. Hara, T. Hiraki, H. Kaino, Y. Kasamatsu, S. Kitao, K. Konashi, Y. Miyamoto, K. Okai, S. Okubo, N. Sasao, M. Seto, T. Schumm, Y. Shigekawa, K. Suzuki, S. Stellmer, K. Tamasaku, S. Uetake, M. Watanabe, T. Watanabe, Y. Yasuda, A. Yamaguchi, Y. Yoda, T. Yokokita, M. Yoshimura, and K. Yoshimura, X-ray pumping of the ^{229}Th nuclear clock isomer, *Nature* **573**, 238 (2019).
- [34] Q. Xiao, G. Penyazkov, R. Yu, B. Huang, J. Li, J. Shi, Y. Yu, Y. Mo, and S. Ding, Proposal for the generation of continuous-wave vacuum-ultraviolet laser light for Th-229 isomer precision spectroscopy, *Phys. Rev. Appl.* **25**, 024034 (2026).
- [35] V. L. Ginzburg, On superconductivity and superfluidity, *Physics–Uspekhi* **47**, 1155 (2004), Nobel Lecture, 8 December 2003.
- [36] E. V. Tkalya, Proposal for a nuclear gamma-ray laser of optical range, *Phys. Rev. Lett.* **106**, 162501 (2011).
- [37] E. V. Tkalya, C. Schneider, J. Jeet, and E. R. Hudson, Radiative lifetime and energy of the low-energy isomeric level in ^{229}Th , *Phys. Rev. C* **92**, 054324 (2015).
- [38] Y. Wang, Y. Yang, Y. Li, D. Yue, K. Zhao, Y. Wang, C. Fu, and Y. Ma, Enhanced yield rate of ^{229m}Th via cascade decay in storage rings and electron beam ion traps (2026), arXiv:2601.22417 [nucl-th].
- [39] F. Schaden, T. Riebner, I. Morawetz, L. T. De Col, G. A. Kazakov, K. Beeks, T. Sikorsky, T. Schumm, K. Zhang, V. Lal, G. Zitzer, J. Tiedau, M. V. Okhupkin, and E. Peik, Laser-induced quenching of the Th-229 nuclear clock isomer in calcium fluoride, *Phys. Rev. Res.* **7**, L022036 (2025).
- [40] C. Zhang, T. Ooi, J. S. Higgins, J. F. Doyle, L. von der Wense, K. Beeks, A. Leitner, G. A. Kazakov, P. Li, P. G. Thirolf, T. Schumm, and J. Ye, Frequency ratio of the ^{229m}Th nuclear isomeric transition and the ^{87}Sr atomic clock, *Nature* **633**, 63 (2024).
- [41] R. Elwell, C. Schneider, J. Jeet, J. E. S. Terhune, H. W. T. Morgan, A. N. Alexandrova, H. B. Tran Tan, A. Derevianko, and E. R. Hudson, Laser excitation of the ^{229}Th nuclear isomeric transition in a solid-state host, *Phys. Rev. Lett.* **133**, 013201 (2024).
- [42] N. Minkov and A. Pálffy, Reduced transition probabilities for the gamma decay of the 7.8 eV isomer in ^{229}Th , *Phys. Rev. Lett.* **118**, 212501 (2017).
- [43] A. M. Dykhne and E. V. Tkalya, Matrix element of the anomalously low-energy (3.5 ± 0.5 eV) transition in ^{229}Th and the isomer lifetime, *Journal of Experimental and Theoretical Physics Letters* **67**, 251 (1998).
- [44] N. Minkov and A. Pálffy, Theoretical predictions for the magnetic dipole moment of ^{229m}Th , *Phys. Rev. Lett.* **122**, 162502 (2019).
- [45] N. Minkov and A. Pálffy, ^{229m}Th isomer from a nuclear model perspective, *Phys. Rev. C* **103**, 014313 (2021).
- [46] Z.-R. Chen, L.-J. Wang, and Y. Wu, Microscopic nuclear structure study of ^{229}Th by projected shell model, *Physics Letters B* **869**, 139858 (2025).
- [47] E. F. Zhou and J. M. Yao, Microscopic study of low-lying states in odd-mass nuclei for atomic electric dipole moment searches (2025), arXiv:2511.05984 [nucl-th].

- [48] N. Minkov, A. Pálffy, P. Quentin, and L. Bonneau, Skyrme-Hartree-Fock-BCS approach to ^{229m}Th and neighboring nuclei, *Phys. Rev. C* **110**, 034327 (2024).
- [49] P. L. Sassarini, J. Dobaczewski, J. Bonnard, and R. F. Garcia Ruiz, Nuclear DFT analysis of electromagnetic moments in odd near doubly magic nuclei, *Journal of Physics G: Nuclear and Particle Physics* **49**, 11LT01 (2022).
- [50] J. Bonnard, J. Dobaczewski, G. Danneaux, and M. Kortelainen, Nuclear DFT electromagnetic moments in heavy deformed open-shell odd nuclei, *Physics Letters B* **843**, 138014 (2023).
- [51] H. Wibowo, B. C. Backes, J. Dobaczewski, R. P. de Groote, A. Nagpal, A. Sánchez-Fernández, X. Sun, and J. L. Wood, Electromagnetic moments in the Sn-Gd region determined within nuclear DFT, *Journal of Physics G: Nuclear and Particle Physics* **52**, 065104 (2025).
- [52] J. Dobaczewski, A. E. Stuchbery, G. Danneaux, A. Nagpal, P. L. Sassarini, and H. Wibowo, Electromagnetic moments of ground and excited states calculated in heavy odd- N open-shell nuclei, *Phys. Rev. C* **113**, 024306 (2026).
- [53] J. Dobaczewski, B. Backes, R. de Groote, A. Restrepo-Giraldo, X. Sun, and H. Wibowo, Electromagnetic and exotic moments in nuclear DFT (2025), submitted to *Annual Review of Nuclear and Particle Science*, arXiv:2511.04632 [nucl-th].
- [54] J. Miśkiewicz, M. Konieczka, and W. Satuła, Two-neutrino $0^+ \rightarrow 0^+$ double- β decay of ^{48}Ca within the density-functional-theory-based no-core configuration-interaction framework, *Phys. Rev. C* **112**, 055502 (2025).
- [55] J. Dobaczewski, P. Bączyk, P. Becker, M. Bender, K. Bennaceur, J. Bonnard, Y. Gao, A. Idini, M. Konieczka, M. Kortelainen, L. Próchniak, A. M. Romero, W. Satuła, Y. Shi, L. F. Yu, and T. R. Werner, Solution of universal nonrelativistic nuclear DFT equations in the Cartesian deformed harmonic-oscillator basis. (IX) HFODD (v3.06h): a new version of the program, *J. Phys. G: Nucl. Part. Phys.* **48**, 102001 (2021).
- [56] J. Dobaczewski *et al.*, Code HFODD, version to be published (2026).
- [57] A. Restrepo-Giraldo *et al.*, Code HFODD, the User Guide, to be published (2026).
- [58] M. Athanasakis-Kaklamanakis, M. Au, A. Kyuberis, C. Zülch, K. Gaul, H. Wibowo, L. Skripnikov, L. Lalanne, J. R. Reilly, A. Koszorús, S. Bara, J. Ballof, R. Berger, C. Bernerd, A. Borschevsky, A. A. Breier, K. Chrysalidis, T. E. Cocolios, R. P. de Groote, A. Dorne, J. Dobaczewski, C. M. Fajardo Zambrano, K. T. Flanagan, S. Franchoo, J. D. Johnson, R. F. Garcia Ruiz, D. Hanstorp, S. Kujanpää, Y. C. Liu, K. M. Lynch, A. McGlone, N. S. Mosyagin, G. Neyens, M. Nichols, L. Nies, F. Pastrana, S. Rothe, W. Ryssens, B. van den Borne, J. Wessolek, S. G. Wilkins, and X. F. Yang, Laser spectroscopy and CP-violation sensitivity of actinium monofluoride, *Nature* **648**, 562 (2025).
- [59] M. Bender, J. Dobaczewski, J. Engel, and W. Nazarewicz, Gamow-Teller strength and the spin-isospin coupling constants of the Skyrme energy functional, *Phys. Rev. C* **65**, 054322 (2002).
- [60] A. Idini, K. Bennaceur, and J. Dobaczewski, Landau parameters for energy density functionals generated by local finite-range pseudopotentials, *Journal of Physics G: Nuclear and Particle Physics* **44**, 064004 (2017).
- [61] B. A. Brown, New Skyrme interaction for normal and exotic nuclei, *Phys. Rev. C* **58**, 220 (1998).
- [62] J. Bartel, P. Quentin, M. Brack, C. Guet, and H.-B. Håkansson, Towards a better parametrisation of Skyrme-like effective forces: A critical study of the SkM force, *Nuclear Physics A* **386**, 79 (1982).
- [63] M. Kortelainen, T. Lesinski, J. Moré, W. Nazarewicz, J. Sarich, N. Schunck, M. V. Stoitsov, and S. Wild, Nuclear energy density optimization, *Phys. Rev. C* **82**, 024313 (2010).
- [64] M. Beiner, H. Flocard, N. V. Giai, and P. Quentin, Nuclear ground-state properties and self-consistent calculations with the Skyrme interaction: (I). Spherical description, *Nuclear Physics A* **238**, 29 (1975).
- [65] P.-G. Reinhard, Skyrme forces and giant resonances in exotic nuclei, *Nucl. Phys. A* **649**, 305c (1999).
- [66] E. Chabanat, P. Bonche, P. Haensel, J. Meyer, and R. Schaeffer, A Skyrme parametrization from subnuclear to neutron star densities Part II. Nuclei far from stabilities, *Nuclear Physics A* **635**, 231 (1998).
- [67] M. Kortelainen, J. McDonnell, W. Nazarewicz, P.-G. Reinhard, J. Sarich, N. Schunck, M. V. Stoitsov, and S. M. Wild, Nuclear energy density optimization: Large deformations, *Phys. Rev. C* **85**, 024304 (2012).
- [68] J. Dobaczewski, J. Engel, M. Kortelainen, and P. Becker, Correlating Schiff moments in the light actinides with octupole moments, *Phys. Rev. Lett.* **121**, 232501 (2018).
- [69] We use the same convention for Q_0^3 as in Ref. [68].
- [70] L. P. Gaffney, P. A. Butler, M. Scheck, A. B. Hayes, F. Wenander, M. Albers, B. Bastin, C. Bauer, A. Blazhev, S. Bönig, N. Bree, J. Cederkäll, T. Chupp, D. Cline, T. E. Cocolios, T. Davinson, H. De Witte, J. Diriken, T. Grahn, A. Herzan, M. Huyse, D. G. Jenkins, D. T. Joss, N. Kesteloot, J. Konki, M. Kowalczyk, T. Kröll, E. Kwan, R. Lutter, K. Moschner, P. Napiorkowski, J. Pakarinen, M. Pfeiffer, D. Radeck, P. Reiter, K. Reynders, S. V. Rigby, L. M. Robledo, M. Rudigier, S. Sambhi, M. Seidlitz, B. Siebeck, T. Stora, P. Thoele, P. Van Duppen, M. J. Vermeulen, M. von Schmid, D. Voulot, N. Warr, K. Wimmer, K. Wrzosek-Lipska, C. Y. Wu, and M. Zielinska, Studies of pear-shaped nuclei using accelerated radioactive beams, *Nature* **497**, 199 (2013).
- [71] H. Wollersheim, H. Emling, H. Grein, R. Kulessa, R. Simon, C. Fleischmann, J. de Boer, E. Hauber, C. Lauterbach, C. Schandera, P. Butler, and T. Czosnyka, Coulomb excitation of ^{226}Ra , *Nuclear Physics A* **556**, 261 (1993).
- [72] F. K. McGowan, C. E. Bemis, W. T. Milner, J. L. C. Ford, R. L. Robinson, and P. H. Stelson, Coulomb excitation of vibrational-like states in the even- A actinide nuclei, *Phys. Rev. C* **10**, 1146 (1974).
- [73] Y. M. Engel, D. M. Brink, K. Goeke, S. J. Krieger, and D. Vautherin, Time-dependent Hartree-Fock theory with Skyrme's interaction, *Nucl. Phys. A* **249**, 215 (1975).
- [74] E. Perlińska, S. G. Rohoziński, J. Dobaczewski, and W. Nazarewicz, Local density approximation for proton-neutron pairing correlations: Formalism, *Phys. Rev. C* **69**, 014316 (2004).
- [75] N. Schunck, *Energy density functional methods for atomic nuclei*, IOP Expanding Physics (IOP Publishing, Bristol, UK, 2019) oCLC: 1034572493.
- [76] P. Ring and P. Schuck, *The nuclear many-body problem*

- (Springer-Verlag, Berlin, 1980).
- [77] J. Dobaczewski, W. Satuła, B. Carlsson, J. Engel, P. Olbratowski, P. Powalowski, M. Sadziak, J. Sarich, N. Schunck, A. Staszczak, M. Stoitsov, M. Zalewski, and H. Zduńczuk, Solution of the Skyrme-Hartree-Fock-Bogolyubov equations in the Cartesian deformed harmonic-oscillator basis.: (VI) HFODD (v2.40h): A new version of the program, *Comput. Phys. Commun.* **180**, 2361 (2009).
 - [78] G. Bertsch, J. Dobaczewski, W. Nazarewicz, and J. Pei, Hartree-Fock-Bogoliubov theory of polarized Fermi systems, *Phys. Rev. A* **79**, 043602 (2009).
 - [79] The dominant Nilsson labels [86] correspond to the largest component of a given s.p. state when it is expanded on the asymptotic Nilsson states $[N_0 n_z \Lambda] \Omega$ [76].
 - [80] J. A. Sheikh, J. Dobaczewski, P. Ring, L. M. Robledo, and C. Yannouleas, Symmetry restoration in mean-field approaches, *Journal of Physics G: Nuclear and Particle Physics* **48**, 123001 (2021).
 - [81] J. Sadoudi, M. Bender, K. Bennaceur, D. Davesne, R. Jodon, and T. Duguet, Skyrme pseudo-potential-based EDF parametrization for spuriousity-free MR EDF calculations, *Physica Scripta* **T154**, 014013 (2013).
 - [82] J. Sadoudi, T. Duguet, J. Meyer, and M. Bender, Skyrme functional from a three-body pseudopotential of second order in gradients: Formalism for central terms, *Phys. Rev. C* **88**, 064326 (2013).
 - [83] K. Bennaceur, A. Idini, J. Dobaczewski, P. Dobaczewski, M. Kortelainen, and F. Raimondi, Nonlocal energy density functionals for pairing and beyond-mean-field calculations, *Journal of Physics G: Nuclear and Particle Physics* **44**, 045106 (2017).
 - [84] See supplemental material at [URL will be inserted by the publisher] for the plots of electromagnetic moments calculated in this Letter.
 - [85] Repository of raw data obtained in this work is available at this URL <https://webfiles.york.ac.uk/HFODD/Projects/229Th..>
 - [86] J. Dobaczewski and J. Dudek, Solution of the Skyrme-Hartree-Fock equations in the Cartesian deformed harmonic oscillator basis II. The program HFODD, *Comput. Phys. Comm.* **102**, 183 (1997).
 - [87] J. A. Sheikh, J. Dobaczewski, P. Ring, L. M. Robledo, and C. Yannouleas, Symmetry restoration in mean-field approaches, *Journal of Physics G: Nuclear and Particle Physics* **48**, 123001 (2021).
 - [88] J. C. Slater, A simplification of the Hartree-Fock method, *Phys. Rev.* **81**, 385 (1951).

End Matter

Convergence and singularities—Our calculations are limited by divergences and singularities arising from the self-interaction and self-pairing properties of the currently available Skyrme functionals [87], which often render solutions unreliable. We were forced to discard such calculations at the mean-field or post-mean-field stages. For the parity-breaking TE and TE+TO calculations, Table I summarizes the properties of the six configurations per functional studied in this Letter.

Skyrme	$\Omega = 5/2$ (TE)			$\Omega = 3/2$ (TE)			$\Omega = 5/2$ (TE+TO)			$\Omega = 3/2$ (TE+TO)						
	$(N_0n_z\Lambda)$	$\overline{(633)}$	$\overline{(752)}$	$\overline{(622)}$	$(N_0n_z\Lambda)$	$\overline{(642)}$	$\overline{(741)}$	$\overline{(631)}$	$(N_0n_z\Lambda)$	$\overline{(633)}$	$\overline{(752)}$	$\overline{(622)}$	$(N_0n_z\Lambda)$	$\overline{(642)}$	$\overline{(741)}$	$\overline{(631)}$
SkX _c	(633)	1(1)	1	1	(642)	1(1)	0	0	(633)	0(0)	0	0	(642)	0(1)	0	0
	(752)	1	1(1)	1	(741)	0	0(1)	0	(752)	0	1(1)	1	(741)	0	0(1)	0
	(622)	1	1	1(1)	(631)	0	0	0(1)	(622)	0	1	1(1)	(631)	0	0	0(1)
SkM*	(633)	0(1)	0	0	(642)	1(1)	0	1	(633)	1(1)	0	0	(642)	1(1)	0	1
	(752)	0	1(1)	0	(741)	0	0(0)	0	(752)	0	0(0)	0	(741)	0	0(0)	0
	(622)	0	0	0(1)	(631)	1	0	1(1)	(622)	0	0	0(1)	(631)	1	0	1(1)
UNEDF1	(633)	0(0)	0	0	(642)	1(1)	0	0	(633)	0(0)	0	0	(642)	0(1)	0	0
	(752)	0	1(1)	0	(741)	0	0(1)	0	(752)	0	1(1)	0	(741)	0	0(1)	0
	(622)	0	0	0(1)	(631)	0	0	0(1)	(622)	0	0	0(1)	(631)	0	0	1(1)
SIII	(633)	0(0)	0	0	(642)	1(1)	0	1	(633)	1(1)	1	1	(642)	0(0)	0	0
	(752)	0	0(1)	0	(741)	0	0(1)	0	(752)	1	1(1)	1	(741)	0	1(1)	1
	(622)	0	0	1(1)	(631)	1	0	1(1)	(622)	1	1	1(1)	(631)	0	1	1(1)
SkO'	(633)	1(1)	0	0	(642)	1(1)	1	1	(633)	0(1)	0	0	(642)	0(0)	0	0
	(752)	0	0(0)	0	(741)	1	1(1)	1	(752)	0	0(0)	0	(741)	0	0(1)	0
	(622)	0	0	0(1)	(631)	1	1	1(1)	(622)	0	0	0(1)	(631)	0	0	0(1)
SLy4	(633)	1(1)	0	1	(642)	1(1)	0	0	(633)	1(1)	0	0	(642)	0(1)	0	0
	(752)	0	0(1)	0	(741)	0	0(1)	0	(752)	0	0(1)	0	(741)	0	0(1)	0
	(622)	1	0	1(1)	(631)	0	0	0(0)	(622)	0	0	0(1)	(631)	0	0	1(1)
UNEDF0	(633)	1(1)	0	1	(642)	1(1)	0	1	(633)	0(1)	0	0	(642)	1(1)	1	0
	(752)	0	0(1)	0	(741)	0	0(1)	0	(752)	0	0(1)	0	(741)	1	1(1)	0
	(622)	1	0	1(1)	(631)	1	0	1(1)	(622)	0	0	1(1)	(631)	0	0	0(0)

TABLE I. Divergences and singularities encountered in the calculations reported in this Letter. Numbers in parentheses, (1) and (0), denote converged and non-converged single-reference solutions, respectively, obtained for the Nilsson labels of the tag states $(N_0n_z\Lambda)$. Numbers without parentheses, 1 and 0, denote non-singular and singular Hamiltonian matrix elements $H_{nn'}^{I+\Omega}$. Boldface entries denote single reference solutions corresponding to the self-consistent Nilsson labels of [633]5/2 or [631]3/2.

Parameters and numerical conditions—We performed the calculations using a 3D harmonic oscillator basis with $N_0 \leq 16$ shells for the harmonic oscillator frequencies [86], $\hbar\omega_0 = 1.2 \times 41 A^{-1/3} = 8.1012$ MeV, and the oscillator length $b = \sqrt{\hbar/m\omega_0} = 2.2625862$ fm, identical in three Cartesian directions.

We used the standard time-even-sector parameters of the Skyrme functionals, as given in the original publications [61–67]. In the time-odd sector, for the UNEDF1, SkO', and SLy4 functionals, the Landau isovector parameters g'_0 were taken from Ref. [49], and for the remaining functionals, they were set to the recommended value of 1.2 [59]. For all functionals, the Landau isoscalar parameters were fixed at 0.4 [59]. The pairing strengths $V_{0,n}$ and $V_{0,p}$ were determined from the mass staggering of neighboring isotopes of ^{229}Th and ^{227}Ac and taken from Ref. [58]. All these parameters are listed in Table II.

In the convention of Ref. [74], the coupling constants of the Skyrme functionals used in this Letter are displayed

in Table III. Values of C_t^s were obtained from the Landau parameters g_0 and g'_0 with $C_t^s[\rho_0] = C_t^s[0]$, where ρ_0 is the nuclear matter saturation density. The Coulomb exchange terms were evaluated within the Slater approximation [88].

Skyrme	g'_0	$V_{0,n}$	$V_{0,p}$	$Q_0^3(^{226}\text{Ra})$	$Q_0^3(^{230}\text{Th})$
SkX _c	1.2	139.02	173.63	0.6654	0.6446
SkM*	1.2	181.47	216.25	1.0763	0.9667
UNEDF1	1.7	145.35	169.79	0.8194	1.0797
SIII	1.2	181.14	220.19	0.8742	2.1131
SkO'	1.0	163.82	184.34	0.9482	1.2839
SLy4	1.3	207.76	231.89	1.0475	1.0088
UNEDF0	1.2	130.61	158.39	0.8887	1.2077

TABLE II. The Landau parameters g'_0 , strengths of the proton and neutron volume pairing interactions, V_p and V_n (in MeV), and intrinsic octupole moments, Q_0^3 (in 1000 fm^3), of ^{226}Ra and ^{230}Th used or calculated in this Letter.

	SkX _c [61]	SkM*[62]	UNEDF1[63]	SIII[64]	SkO'[65]	SLy4[66]	UNEDF0[67]
C_0^ρ	-539.250000	-991.875000	-779.373009	-423.281250	-787.282125	-933.341250	-706.382929
C_1^ρ	283.286000	390.137500	287.722131	268.078125	246.942585	830.051485	240.049522
C_0^s	44.138239	38.905862	30.554818	41.584341	219.237417	44.243392	34.079267
C_1^s	135.000706	116.717587	129.857975	124.753022	101.970111	143.791024	102.237800
C_0^τ	-0.821625	34.687500	-0.989914	44.375000	15.000072	57.129375	-12.917242
C_1^τ	-44.706725	-34.062500	-33.632096	-30.625000	-4.156240	24.656385	-45.189417
C_0^T	-7.389900	0.000000	0.000000	0.000000	-104.093563	0.000000	0.000000
C_1^T	-23.625000	0.000000	0.000000	0.000000	-9.171875	0.000000	0.000000
C_0^J	0.821625	-34.687500	0.989914	-44.375000	-15.000072	-57.129375	12.917242
C_1^J	44.706725	34.062500	33.632096	30.625000	4.156240	-24.656385	45.189417
C_0^J	7.389900	0.000000	0.000000	0.000000	104.093563	0.000000	0.000000
C_1^J	23.625000	0.000000	0.000000	0.000000	9.171875	0.000000	0.000000
$C_0^{\Delta\rho}$	-46.011656	-68.203125	-45.135131	-62.968750	-52.787044	-76.996406	-55.260600
$C_1^{\Delta\rho}$	22.750481	17.109375	-145.382168	17.031250	-32.162034	15.657086	-55.622600
$C_t^{\Delta s}, C_t^{\nabla s}$	0.000000	0.000000	0.000000	0.000000	0.000000	0.000000	0.000000
$C_0^{\nabla J} = C_0^{\nabla j}$	-72.850000	-97.500000	-74.026333	-90.000000	-102.450600	-92.250000	-79.530800
$C_1^{\nabla J} = C_1^{\nabla j}$	0.000000	-32.500000	-35.658261	-30.000000	41.444400	-30.750000	45.630200

TABLE III. Unrounded coupling constants of the Skyrme functionals used in this Letter.

Results in numerical form—In Table IV, we show the unrounded numerical values of the $B(M1:3/2_1^+ \rightarrow 5/2_1^+)$ transition probabilities (in μ_N^2), spectroscopic magnetic dipole moments μ (in μ_N), and spectroscopic electric quadrupole moments Q (in barn) calculated for the mixed, not mixed, and no-octupole $5/2^+$ and $3/2^+$ states. The upper, middle, and lower groups of rows correspond to the left, center, and right panels of Fig. 4. Values and uncertainties obtained from the regression analysis relative to the ^{226}Ra and ^{230}Th data are also shown. Values without uncertainties correspond to a two-point regression. The last row lists the experimental data [6, 21, 28].

		B(M1)		$\mu(5/2^+)$		$Q(5/2^+)$		$\mu(3/2^+)$		$Q(3/2^+)$	
Skyrme		TE	TE+TO	TE	TE+TO	TE	TE+TO	TE	TE+TO	TE	TE+TO
MIXED	SkX _c	0.01026	—	-0.79535	0.41030	2.7726	2.8080	0.51042	—	1.5391	—
	SkM*	0.04508	0.07176	-0.36250	0.55101	3.0054	2.9568	-0.16870	-0.01990	1.7135	1.7154
	UNEDF1	0.05547	0.04833	-0.12505	0.25525	3.0628	3.0642	0.21499	-0.26823	1.6418	1.6953
	SIII	0.32901	0.06880	-0.69481	0.96563	2.6864	2.8825	-0.51371	-0.15283	1.6143	1.5379
	SkO'	0.07900	—	0.86083	—	3.0198	—	-0.49344	—	1.6320	—
	SLy4	0.03430	0.00456	-0.38997	0.31410	2.9714	2.9926	0.40281	-0.32877	1.5991	1.6756
	UNEDF0	0.00377	0.00588	0.69722	-0.13349	3.0010	3.0328	0.78717	-0.23921	1.6769	1.6790
	^{226}Ra regression	0.08(8)	0.04(3)	0.0(4)	0.4(3)	3.01(9)	3.01(7)	-0.1(3)	-0.1(1)	1.68(3)	1.69(6)
^{230}Th regression	-0.01(3)	0.03(2)	-0.2(3)	0.2(2)	2.98(7)	2.96(6)	0.4(2)	-0.2(1)	1.62(3)	1.73(1)	
NOT MIXED	SkX _c	—	—	0.27118	—	2.9095	—	—	—	—	—
	SkM*	—	0.07380	—	0.55101	—	2.9568	-0.18195	-0.09812	1.7133	1.7149
	UNEDF1	—	—	—	—	—	—	—	-0.26823	—	1.6953
	SIII	—	0.02179	—	0.79171	—	2.8937	-0.54818	-0.38116	1.6141	1.6141
	SkO'	0.06019	—	0.86083	—	3.0198	—	-0.57155	—	1.6835	—
	SLy4	—	0.00456	0.19361	0.31410	2.9984	2.9926	—	-0.32877	—	1.6756
	UNEDF0	0.00145	—	0.50012	—	2.9168	—	0.16136	-0.24113	1.6904	1.6789
	^{226}Ra regression	0.19	0.04(4)	0.5(3)	0.4(2)	3.01(4)	2.98(3)	-0.3(4)	-0.2(1)	1.72(4)	1.69(3)
^{230}Th regression	-0.31	0.04(4)	0.3(2)	0.4(1)	2.94(4)	2.99(2)	-0.1(3)	-0.19(6)	1.73(3)	1.73(2)	
NO OCTUPOLE	SkX _c	0.07804	0.09297	0.83200	0.63589	2.9140	2.9127	-0.46792	-0.31471	1.6240	1.6234
	SkM*	0.20008	0.19810	0.70337	0.55873	2.9561	2.9565	0.21260	0.18240	1.7166	1.7165
	UNEDF1	0.33397	—	0.18417	0.17797	3.0287	3.0285	-0.10385	-0.03062	1.7125	1.7118
	SIII	0.06343	0.06659	0.89248	0.71634	2.8973	2.8964	-0.51329	-0.35483	1.6143	1.6137
	SkO'	0.05298	0.08053	0.95830	0.74518	3.0210	3.0165	-0.57189	-0.41960	1.6814	1.6809
	SLy4	0.20014	0.20001	0.39101	0.36633	2.9840	2.9852	-0.28603	-0.18165	1.6829	1.6829
	UNEDF0	0.26571	0.25370	0.50392	0.45116	2.9129	2.9156	0.16926	0.16695	1.6952	1.6952
	^{226}Ra regression	0.19(8)	0.19(5)	0.6(2)	0.5(1)	2.98(4)	2.98(4)	-0.1(2)	-0.0(2)	1.70(2)	1.70(2)
^{230}Th regression	0.20(6)	0.17(4)	0.6(2)	0.5(1)	2.97(3)	2.97(3)	-0.1(2)	-0.1(1)	1.69(2)	1.69(2)	
Experiment	0.0388(12)		0.366(6)		3.11(2)		-0.378(8)		1.77(1)		

TABLE IV. Unrounded numerical values of results determined in this Letter, see text.

Supplemental Material for: Radiative decay and electromagnetic moments in ^{229}Th determined within nuclear DFT

A. Restrepo-Giraldo¹, J. Dobaczewski^{1,2}, J. Bonnard¹ and X. Sun¹

¹*School of Physics, Engineering and Technology,
University of York, Heslington, York YO10 5DD, United Kingdom*

²*Institute of Theoretical Physics, Faculty of Physics,
University of Warsaw, ul. Pasteura 5, PL-02-093 Warsaw, Poland*

(Dated: February 17, 2026)

Using the nuclear DFT approach with symmetry breaking and restoration, we investigate the electromagnetic properties of the ground and isomeric states in ^{229}Th . We determine the magnetic dipole transition strength $B(M1:3/2_1^+ \rightarrow 5/2_1^+)$ between these two states and discuss the effects of parity breaking, configuration mixing, and time-odd core polarization. We also determine the corresponding spectroscopic magnetic dipole and electric quadrupole moments. Because the octupole deformability of the Skyrme functionals used here is not described in sufficient detail, we analyze the results using a set of Skyrme functionals, implementing a regression aligned with the measured octupole moments of neighboring even-even nuclei. Without parameter adjustment, the results compare favorably with the experimental data but also indicate the need to systematically adjust the octupole degrees of freedom in future functional parametrizations.

Plots of electromagnetic moments—Figures 5–10 show the results of the regression analysis for the magnetic dipole moments (Figs. 5–7) and electric quadrupole moments (Figs. 8–10) of the $3/2^+$ isomeric and $5/2^+$ ground states, and for the TE and TE+TO variants of calculations. Figures 5 and 8, analogous to Fig. 1, show the results for parity breaking and mixing of configurations, where the numbers in parentheses represent the number of configurations mixed to obtain the results. Figures 6 and 9, analogous to Fig. 2, show the results for parity breaking with no mixing, while Figs. 7 and 10, analogous to Fig. 3, display the result for the parity-conserving variant with no mixing.

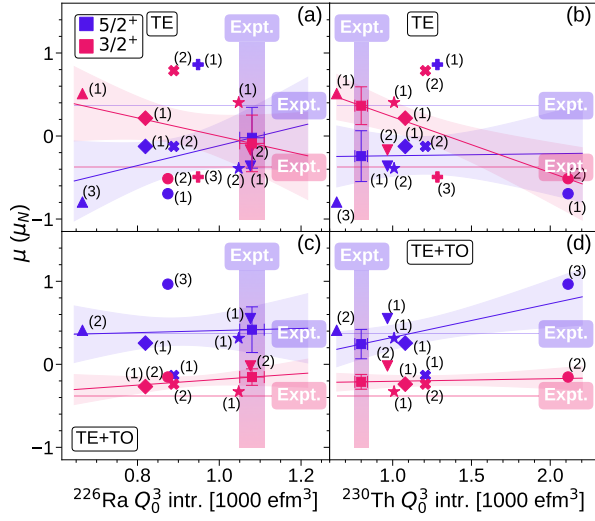


FIG. 5. Same as Fig. 1 but for magnetic dipole moments.

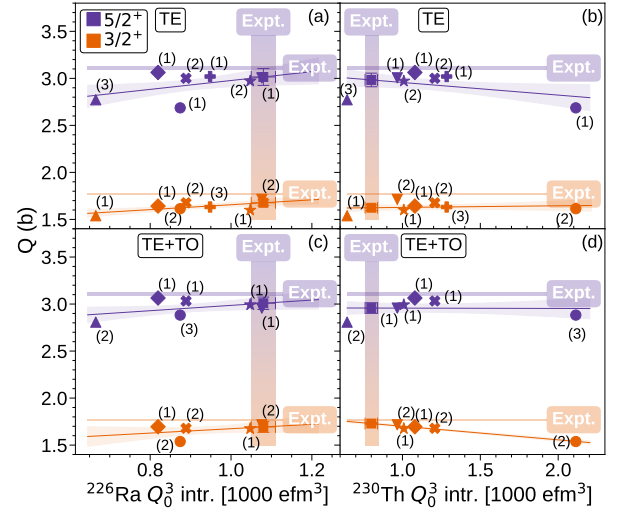


FIG. 8. Same as Fig. 1 but for electric quadrupole moments.

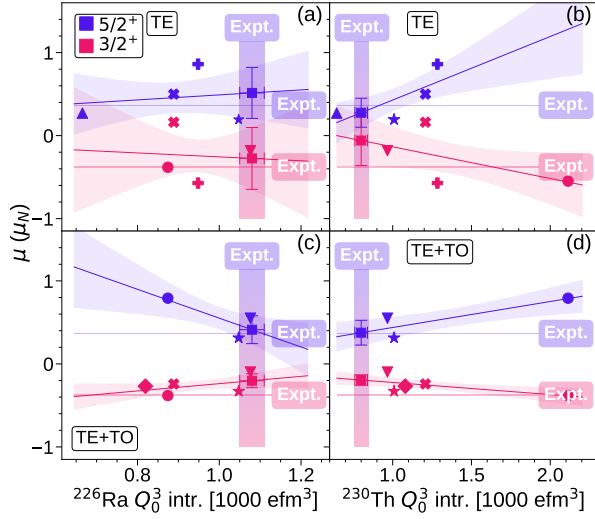


FIG. 6. Same as Fig. 2 but for magnetic dipole moments.

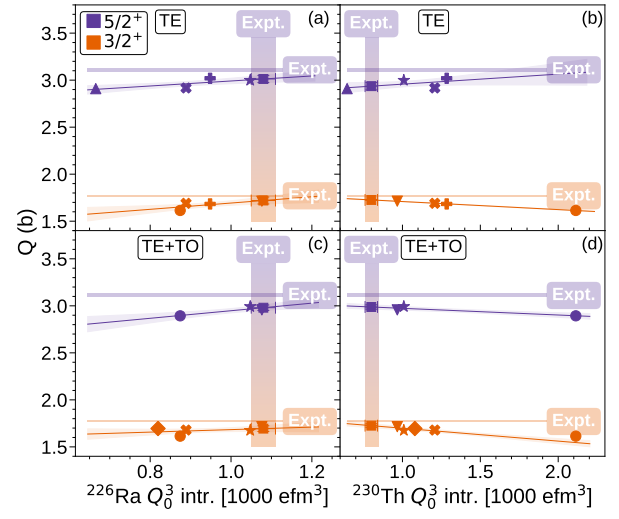


FIG. 9. Same as Fig. 2 but for electric quadrupole moments.

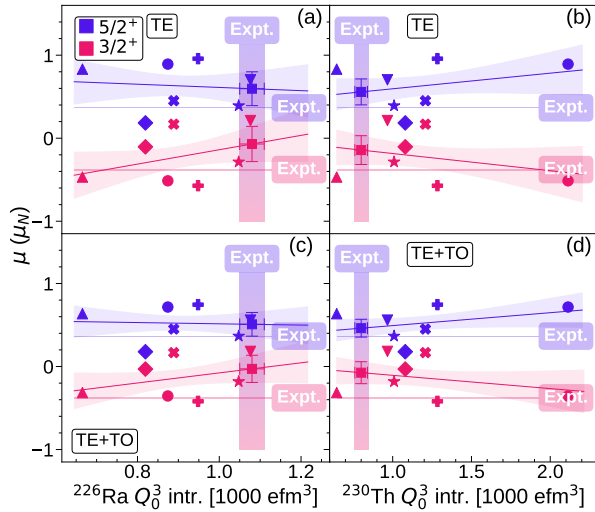


FIG. 7. Same as Fig. 3 but for magnetic dipole moments.

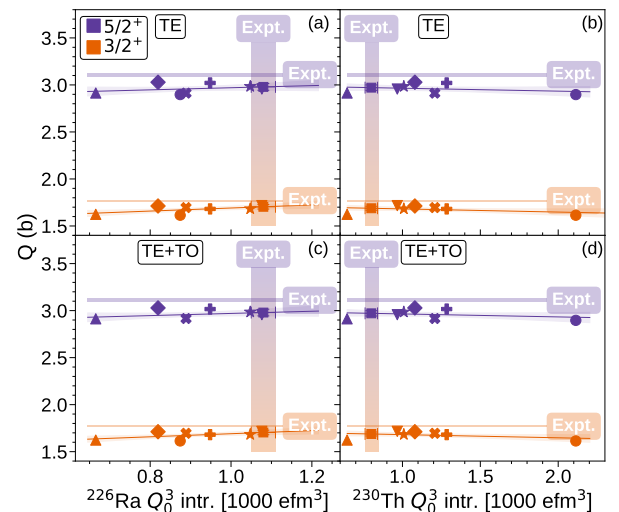


FIG. 10. Same as Fig. 3 but for electric quadrupole moments.